$[Fe^{II}(L^{\bullet})_2][TCNQF_4^{\bullet -}]_2$: A Redox-active Double Radical Salt.

Ian A. Gass,*[a,b] Jinzhen Lu,[a] Ruchika Ojha,[a] Mousa Asadi,[a] David W. Lupton,[a] Blaise L. Geoghegan,[b] Boujemaa Moubaraki,[a] Lisandra L. Martin,[a] Alan M. Bond,[a] and Keith S. Murray*[a]

[a]School of Chemistry, Monash University, Clayton, Victoria 3800, Australia.

[b]School of Pharmacy and Biomolecular Sciences, University of Brighton, Brighton BN2 4GJ, UK

Abstract

The reaction of $[Fe^{II}(L^{\bullet})_2][BF_4]_2$ with $LiTCNQF_4$ results in the formation of $[Fe^{II}(L^{\bullet})_2][TCNQF_4^{\bullet-}]_2 \cdot 2CH_3CN$ (**1**) ($L^{\bullet}$ is the neutral aminoxyl radical ligand, 4,4-dimethyl-2,2-di(2-pyridyl)oxazolidine-N-oxide; $TCNQF_4$ is 2,3,5,6-tetrafluoro-7,7,8,8-tetracyanoquinodimethane). Single crystal X-ray diffraction; Raman, Fourier transform infrared (FTIR) and ultraviolet-visible (UV-Vis) spectroscopies; and electrochemical studies are all consistent with the presence of: a low-spin Fe^{II} ion; the neutral radical form ($L^{\bullet}$) of the ligand; and the radical anion, $TCNQF_4^{\bullet-}$. **1** is largely diamagnetic and the electrochemistry shows five well resolved, diffusion-controlled, reversible, one electron processes.

Introduction

Much of the initial interest in the interaction of metal ions and redox active ligands stemmed from their biological relevance,[1] sparking an ongoing debate on the exact structure in the diamagnetic, oxygen binding proteins, oxymyoglobin and oxyhemoglobin. Weiss argued for a structure containing strong antiferromagnetic exchange between low-spin Fe(III) and a superoxide anion ($Fe^{III}/O_2^{\bullet -}$)[2] while Pauling advocated for a combination of low-spin Fe(II) and singlet oxygen (Fe^{II}/O_2^{0}).[3] Later studies, of course, revealed a more complex situation involving non-standard effective nuclear charges , spin polarization effects and partial metal character of ligand based orbitals[4] but this example highlights the importance of characterising such interactions fully and paying close attention to the electronic structure associated with the metal ion in such systems. Similarly the active site of catechol dioxygenases, responsible for intra-diol cleavage, contains iron ions with the catecholate/o-quinone redox system[5–7] and the tyorsyl/tyrosinate redox pair is used in combination with manganese in photosystem II,[8] copper in galactose oxidase,[9] and iron in ribonucleotide reductase.[10] The multi-electron processes present in such metalloenzymes have molecular equivalents and are utilised in aerobic alcohol oxidation catalysts which are chemoselective, tolerant of the presence of other functional groups and use atmospheric molecular oxygen as the oxidant.[11–13] Similar transition metal/redox active ligand species can also potentially mimic the multi-electron processes of the more expensive, and rarer, noble metals offering a pathway to catalysts made out of cheaper, and more abundant, metals such as iron.[14] In addition to the bioinorganic perspective and catalysis work detailed above our initial interest in these systems was spurred on by the “metal-radical” approach pioneered by Gatteschi and

co-workers[15,16] with an emphasis on studying the effects of coordinated radicals on spin-crossover and single-molecule magnet behaviour.[17–22]

The recently reported redox congener pairs, $[M^{II}(L^{\bullet})_2]^{2+}$ / $[M^{III}(L^{-})_2]^{+}$ (M = Fe, Co and L^{-} = reduced form of $L^{\bullet}$)[17–20] show multiple redox processes and can be easily converted between their two forms by either chemical or electrochemical means. They show a range of interesting physical behaviour including reductively induced oxidation, spin-crossover and field-induced single-molecule magnet behaviour.[17–20] The switchable nature of these cations has led us to prepare a range of multifunctional materials using anions such as the $[Re^{IV}X_6]^{2-}$ anion (X = Cl, Br) which showed spin-canting behaviour in $[Ni^{II}(L^{\bullet})(H_2O)_3][Re^{IV}Cl_6]$ and the only example to date of a single radical ligand ($L^{\bullet}$) coordinating facially around a central metal ion.[22]

Initial work on combining $[Fe^{II}(L^{\bullet})_2](BF_4)_2$[17] with the $TCNQF_4^{2-}$ anion resulted in the $TCNQF_4^{2-}$ anion acting as a reducing agent towards the $[Fe^{II}(L^{\bullet})_2]^{2+}$ cation converting it to $[Fe^{III}(L^{-})_2]^{+}$ via a reductively induced oxidation process. The $TCNQF_4^{2-}$ dianion was subsequently oxidised to its anionic radical form, $TCNQF_4^{\bullet -}$, which then crystallised as $[Fe^{III}(L^{-})_2][TCNQF_4^{\bullet -}]$.[23] To confirm our initial hypothesis that the $TCNQF_4^{2-}$ species was solely responsible for the reductively induced oxidation of $[Fe^{II}(L^{\bullet})_2]^{2+}$ in this work we performed a similar reaction but using the monoanionic radical salt, $LiTCNQF_4$, instead of Li_2TCNQF_4. This should result in a simple salt metathesis replacing the two BF_4^{-} anions with two $TCNQF_4^{\bullet -}$ radical anions and generate a new related redox active species. By addition of two equivalents of $LiTCNQF_4$ in methanol to a solution of $[Fe^{II}(L^{\bullet})_2][BF_4]_2$[17], pre-dissolved in a mixture of acetonitrile and dichloromethane, crystalline product of $[Fe^{II}(L^{\bullet})_2][TCNQF_4^{\bullet -}]_2{\cdot}2CH_3CN$ (**1**) was indeed obtained in 69% yield (Fig. 1).

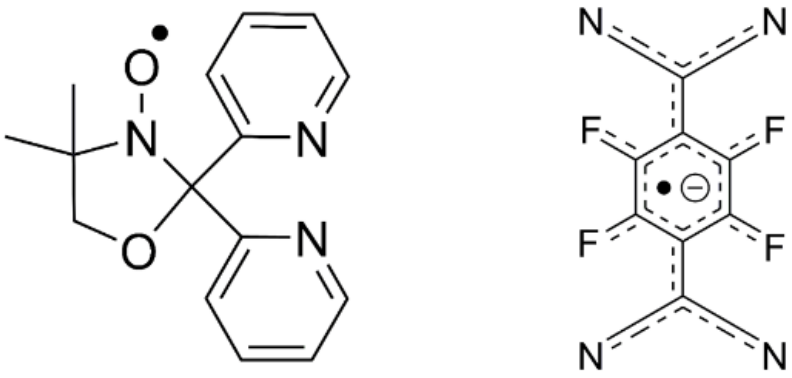

Fig. 1. Structural formula of L• (top left) and $TCNQF_4$•- (top right).

Results and Discussion

Synthesis and Structure

Complex **1** crystallises in the monoclinic space group *C*2/c with the asymmetric unit containing half the $[Fe^{II}(L^{\bullet})_2]^{2+}$ dication, one $TCNQF_4^{\bullet-}$ radical anion and one solvate acetonitrile molecule (Figs. 2-3). An inversion centre sits on the central iron ion in **1** which generates the $[Fe^{II}(L^{\bullet})_2]^{2+}$ monocation which is then charge balanced by two $TCNQF_4^{\bullet-}$ radical anions and accompanied by two solvate acetonitriles as per the formula; $[Fe^{II}(L^{\bullet})_2][TCNQF_4\bullet-]_2{\cdot}2CH_3CN$ (**1**). Relevant bond lengths and angles for the $[Fe^{II}(L^{\bullet})_2]^{2+}$ dication, as well as a comparison with $[Fe^{II}(L^{\bullet})_2][BF_4]_2$ can be found in Table 1 and selected geometric parameters for the $TCNQF_4^{\bullet-}$ radical anions can be found in Table 2.

In **1** two tridentate nitroxide radical ligands coordinate to the central Fe ion axially via the oxygen and equatorially via the pyridyl nitrogen groups from each ligand resulting in a distorted octahedral geometry with the following parameters: cis angles, 87.76(7) – 92.24(7)°; trans angles, 180°; Fe-O = 1.89 Å, Fe-N = 1.96 and 1.98 Å (full bond lengths with errors can be found in the CIF file). The intramolecular ($L^{\bullet}$ to $L^{\bullet}$) distance in **1** is 5.20 Å. This intramolecular distance was between calculated centroids of the nitroxide N-O group. In **1** there are two $TCNQF_4^{\bullet-}$ radical anions, in dimeric form, present per $[Fe^{II}(L^{\bullet})_2]^{2+}$ dication (Figs. 2-3).

Assigning the oxidation and spin states of the $[Fe^{II}(L^{\bullet})_2]^{2+}$ dication and confirmation of both the $[TCNQF_4]^{\bullet-}$ radical anion and the neutral radical form of the ligand $L^{\bullet}$, is well established and relies on a rigorous examination of the bond lengths and angles contained in both the cation[17–23] and anion[24–26] (Tables 1-3). The nitroxide N-O (N3-O1) bond length is 1.30 Å in **1** which strongly suggests the ligand ($L^{\bullet}$) is in the neutral radical form as found previously when relating nitroxide bond lengths to the redox form of the NO group.[17–23] Equally the

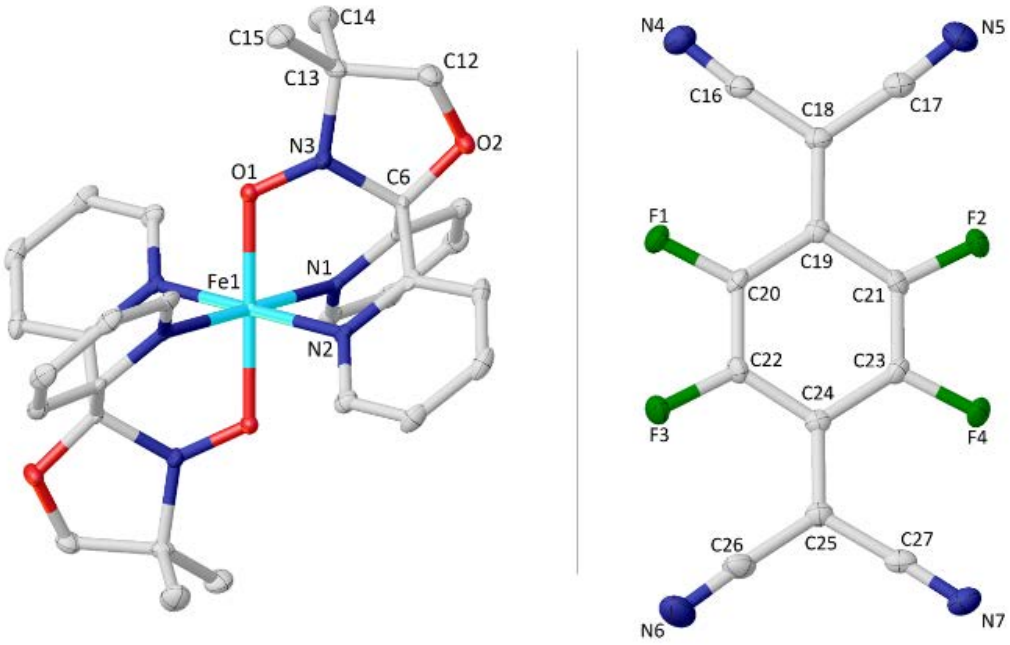

Fig. 2. Molecular structure of the dication $[Fe^{II}(L^{\bullet})_2]^{2+}$ (left) and the $TCNQF_4^{\bullet-}$ radical anion (right). Colour code: Fe, turquoise; O, red; N, blue; C; grey ; F, green.

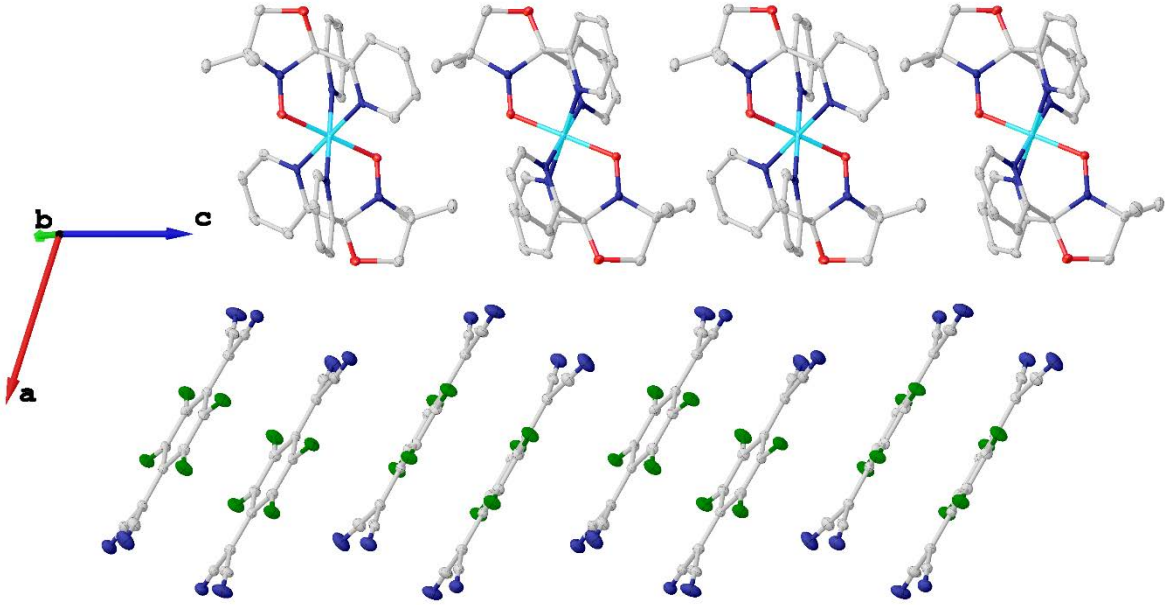

Fig. 3 Packing diagram of **1** showing the arrangement of $[Fe^{II}(L^{\bullet})_2]^{2+}$ dications and pairs of eclipsed $TCNQF_4^{\bullet-}$ radical anions. Colour code: Fe, turquoise; O, red; N, blue; C; grey ; F, green.

Table 1 Selected bond lengths (Å) and angles (°) for the dication, $[Fe^{II}(L^{\bullet})_2]^{2+}$, in **1** and the corresponding bond length and angles for the dication, $[Fe^{II}(L^{\bullet})_2]^{2+}$, in $[Fe^{II}(L^{\bullet})_2][BF_4]_2$.[17] Full bond lengths with errors can be found in the CIF file.

Geometric parameters	**1** (123 K)	$[Fe^{II}(L^{\bullet})_2][BF_4]_2$[a]
O(1)-N(3)	1.30	1.32 / 1.31
Fe(1)-O(1)	1.89	1.88 / 1.88
Fe(1)-N(1)	1.96	1.97 / 1.96
Fe(1)-N(2)	1.98	1.98 / 1.99
N(3)-C(6)	1.47	1.47 / 1.47
N(3)-C(13)	1.47	1.47 / 1.48
C(6)-O(2)	1.40	1.40 / 1.39
O(2)-C(12)	1.44	1.44 / 1.45
C(12)-C(13)	1.53	1.54 / 1.52
C(13)-C(14)	1.52	1.52 / 1.54
C(13)-C(15)	1.52	1.51 / 1.51
Fe(1)-O(1)-N(3)	116.35(12)	117.58(16) / 117.50(16)
Fe(1)-O(1)-N(3)-C(6)[b]	14.006	13.973 / -14.298
Fe(1)-O(1)-N(3)-C(13)[b]	171.762	166.036 / -164.474
O(1)-N(3)-C(6)-C(13)[b]	160.115	154.875 / -153.514

[a] There are two crystallographically unique dications in $[Fe^{II}(L^{\bullet})_2][BF_4]_2$ hence the two numbers. These are corresponding bond lengths and angles only and the second cation of $[Fe^{II}(L^{\bullet})_2][BF_4]_2$ will not have identical atom numbering as in **1**. [b] For a system with four atoms A, B, C, D the torsion angle A-B-C-D will be the angle formed between the plane formed by A, B and C and the plane formed between B, C and D. The sign of the torsion angle is positive if the bond A-B is rotated in a clockwise direction through less than 180° in order that it may eclipse the bond C-D: a negative torsion angle requires rotation in the opposite sense.

Table 2 Selected bond lengths (Å) and angles (°) for the anionic radical $TCNQF_4^{\bullet -}$ in **1**. Full bond lengths with errors can be found in the CIF file.

Bond lengths	**1** (123 K) $TCNQF_4^{\bullet -}$
N(4)-C(16)	1.15
N(5)-C(17)	1.15
C(16)-C(18)	1.42
C(17)-C(18)	1.42
C(18)-C(19)	1.42
C(19)-C(20)	1.41
C(19)-C(21)	1.42
F(1)-C(20)	1.34
F(2)-C(21)	1.34
C(20)-C(22)	1.35
C(21)-C(23)	1.36
F(3)-C(22)	1.34
F(4)-C(23)	1.34
C(22)-C(24)	1.41
C(23)-C(24)	1.41
C(24)-C(25)	1.41
C(25)-C(26)	1.43
C(25)-C(27)	1.42
N(6)-C(26)	1.15
N(7)-C(27)	1.15

Table 3 Calculation of the charge transfer degree ρ using C-C and C=C mean bond lengths; b,c and d as designated below.

Species	**b**	**c**	**d**	ρ
1	1.413	1.415	1.423	-0.98
$TCNQF_4$	1.437	1.372	1.437	0
$(n\text{-}Bu_4N)[TCNQF_4^{\bullet -}]$	1.417	1.418	1.426	-1.00
$(X)_2(TCNQF_4^{2-})$	1.386	1.461	1.393	-2.21

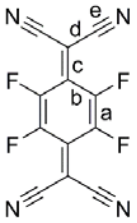

$\rho = A(c/(b+d)) + B$ where A = -45.756 and B = 21.846 which are calculated from $TCNQF_4$ and $[TCNQF_4]^{\bullet -}$ assuming $\rho = 0$ for the neutral $TCNQF_4$ moiety and $\rho = -1$ for the anionic radical form in $[TCNQF_4]^{\bullet -}$. The values in Table 3 are taken from $TCNQF_4$[24], $(n\text{-}Bu_4N)[TCNQF_4^{\bullet -}]$[25] and $(X)_2(TCNQF_4^{2-})$[27] where X = 1,4-dibenzyl-1,4-diazabicyclo[2.2.2]octane-1,4-diium. Average bond length values have been taken throughout.

Fe-O (1.89 Å) and Fe-N (1.96 and 1.98 Å) bond lengths are indicative of a central low-spin Fe(II) ion. If we look at the geometry around N3 then this results in a small deviation from the plane formed by O1-C6-C13 (Table 1). This is expected considering the resonance forms of the neutral radical form of the ligand ($L^{\bullet}$) where we do not have a localised lone pair on N3 and hence would expect a trigonal planar arrangement around N3. This is in comparison to the trigonal pyramidal geometry found when the ligand is in the hydroxylamino anionic form, L^{-}.[23] The cationic species in **1** are therefore assigned as $[Fe^{II}(L^{\bullet})_2]^{2+}$ where the Fe^{II} ion is in the low-spin state. From charge balance considerations alone then the $TCNQF_4$ species in **1** must be the $TCNQF_4^{\bullet-}$ radical anion given that **1** has two $TCNQF_4$ moieties as anions. As the charge of the $TCNQF_4$ moiety increases the bond length labelled c (Table 3) increases in length while b and d decrease in length. The charge transfer degree of the $TCNQF_4$ moiety (ρ) can be then be calculated by the Kistenmacher relationship[9] (Table 3). The calculated ρ values are -0.98 for **1** suggesting that $TCNQF_4$ moieties in **1** are $TCNQF_4^{\bullet-}$ radical anions. This leads to the assignment of **1** as $[Fe^{II}(L^{\bullet})_2][TCNQF_4^{\bullet-}]_2 \cdot 2CH_3CN$.

1 consists of alternating layers of $[Fe^{II}(L^{\bullet})_2]^{2+}$ cations and pairs of eclipsed $TCNQF_4^{\bullet-}$ radical anions (Fig. 3) with an interplanar distance of 3.28 Å (based on distance between calculated centroids of the planes of the six-member ring of the $TCNQF_4^{\bullet-}$ radical anion). No significant intermolecular interactions were found anywhere else in the structure and the shortest intermolecular distances are 7.86 Å (Fe to Fe), 5.20 Å ($L^{\bullet}$ to $L^{\bullet}$) and 6.32 Å (Fe to $L^{\bullet}$) where distances were based on calculated centroids of the nitroxide N-O group. The solvate acetonitrile groups are not involved in any significant intermolecular interactions with the

acetonitrile orientated parallel to the pyridine ring of the ligand associated with N2 (Figs. S1-S2).

Raman and FTIR spectroscopy

Raman and Infrared spectroscopic studies can be used to confirm the assignment of the $TCNQF_4^{\bullet-}$ radical anion in **1**.[26,28] In Raman spectroscopy the most important diagnostic stretch is the C≡N stretch which occurs at 2226 cm^{-1} for neutral $TCNQF_4^0$ and this occurs at 2220 cm^{-1} in **1** (Fig. S3). We would expect the C≡N to shift to lower energies in the $TCNQF_4^{\bullet-}$ radical anion compared to neutral $TCNQF_4^0$ and is consistent with $LiTCNQF_4$ whose C≡N band is at 2223 cm^{-1} (Fig. S4). Additional diagnostic modes in the Raman spectra are: the ring C=C stretch at 1643 cm^{-1} which is consistent with the $TCNQF_4^{\bullet-}$ radical anion; and the exocyclic C=C stretch which is expected at around 1445 cm^{-1} but is either absent or significantly shifted to 1392 cm^{-1} in **1**. The FTIR spectrum for **1** is shown in Fig. S5 with two C≡N stretches observed at 2194 and 2173 cm^{-1} which again are shifted to lower wavenumbers than those found in neutral $TCNQF_4^0$ (2225 cm^{-1}).[26] Further diagnostic modes in the infrared spectra can be found at: 1536 cm^{-1} corresponding to a ring C=C stretch; 1505 cm^{-1} corresponding to an exocyclic C=C stretch; and 1346 cm^{-1} corresponding to a C-F and ring C-C stretch. Overall the diagnostic modes detailed above are characteristic of the $TCNQF_4^{\bullet-}$ radical anion. A full treatment of the vibrational spectroscopy of different redox forms of $TCNQF_4$ has been reported previously.[28]

Magnetic Studies

DC magnetic susceptibilities were performed on crystals of **1** in the 2 – 300 K range under an applied field of 0.1 T (Fig. S6). Complex **1** has only small residual $\chi_M T$ values ranging from 0.08 $cm^3\ mol^{-1}\ K$ at 300 K to 0.07 $cm^3\ mol^{-1}\ K$ at 2 K. The previously reported[17] $[Fe^{II}(L^{\bullet})_2]^{2+}$

dicationic complex showed strong radical-radical antiferromagnetic interactions mediated by the Fe^{2+} centre resulting in a $S = 0$ ground state and stacked pairs of eclipsed $TCNQF_4^{\bullet -}$ radical anions are known to exhibit strong antiferromagnetic interactions.[29] A comparison of the $\chi_M T$ vs T plots for **1** and $[Fe^{II}(L^{\bullet})_2][BF_4]_2$ shows a similar profile above 150 K (Fig. S7) and the bond lengths and angles of the $[Fe^{II}(L^{\bullet})_2]^{2+}$ dication in **1** are similar to that observed in $[Fe^{II}(L^{\bullet})_2][BF_4]_2$ (Table 2). It is reasonable to suggest that a similar radical-radical antiferromagnetic interaction occurs in the $[Fe^{II}(L^{\bullet})_2]^{2+}$ dication in **1** although the shallower slope of the $\chi_M T$ vs T plot (Figs. S7-S8) suggests a slightly stronger antiferromagnetic interaction in **1** compared to that seen in $[Fe^{II}(L^{\bullet})_2][BF_4]_2$. Using the program PHI[30] a reasonable simulation of the data in **1** from 150 K to 300 K was calculated using a $S = 1/2$ dimer model with the isotropic spin Hamiltonian, $\hat{H} = -2J\hat{S}_1 \cdot \hat{S}_2$ and parameters $g = 2.00$ and $J = -380$ cm^{-1} (Fig. S8). This is slightly stronger than the equivalent interaction in $[Fe^{II}(L^{\bullet})_2][BF_4]_2$ ($J = -315$ cm^{-1}) but is consistent with the overall expectation of a large radical-radical antiferromagnetic interaction between the two radical ligands mediated by the central, and low-spin, Fe(II) ion. This seems reasonable but this analysis is dependent on the assumption that the pairs of eclipsed $TCNQF_4^{\bullet -}$ radical anions are so strongly coupled that their contribution to the $\chi_M T$ vs T plot is negligible across the temperature range studied. This appears to be the case for the data above 150 K, but there is a small increase in $\chi_M T$ values from 150 K to 2K resulting in a final value of 0.07 cm^3 mol^{-1} K at 2 K (Fig. S6-S8), the origin of which is clearly not from the $[Fe^{II}(L^{\bullet})_2]^{2+}$ dication, the $TCNQF_4^{\bullet -}$ radical anions or any temperature independent paramagnetism (TIP). In $[Fe^{II}(L^{\bullet})_2][BF_4]_2$[17] there was evidence of the presence of 5% of a species containing low-spin Fe(III) and a neutral radical ligand; likely to be the $[Fe^{III}(L^{\bullet})(L^{-})]^{2+}$ dication. It is possible that the $\chi_M T$ values below 150 K are simply the

result of either intramolecular/intermolecular interactions of this minor, or related, species. Overall, and noting the data below 150 K, the observed $\chi_M T$ vs T plot is therefore reasonable given the assignment of **1** as $[Fe^{II}(L^{\bullet})_2][TCNQF_4^{\bullet -}]_2 \cdot 2CH_3CN$.

Solution phase studies on dissolved solid $[Fe^{II}(L^{\bullet})_2][TCNQF_4^{\bullet -}]_2$

UV-Vis Studies

The solid state studies above show that the crystallography, microanalysis and Raman / FTIR spectroscopies are consistent with the assignment of **1** as $[Fe^{II}(L^{\bullet})_2][TCNQF_4^{\bullet -}]_2 \cdot 2CH_3CN$ where the central Fe(II) ion is low-spin, the ligands are in the neutral radical form ($L^{\bullet}$) and we have two eclipsed $TCNQF_4^{\bullet -}$ radical anions. Solution studies for **1** were then undertaken in acetonitrile (~ 0.1 mM) with the UV-vis spectra shown in Fig. S9 showing two intense absorption bands with λ_{max} at 411 and 753 nm which are characteristic for the $TCNQF_4^{\bullet -}$ radical anion[26] and a minor absorption band at 247 nm was observed, corresponding to the neutral radical form ($L^{\bullet}$) of the ligand (Fig. S10). This confirms that the solid state structure and subsequent redox levels of the cation and anion remain intact in solution.

Electrochemistry

The dissolution of **1** in acetonitrile gives an emerald green solution. A transient cyclic voltammogram of a 0.35 mM solution of **1** at a glassy carbon (GC) macrodisc electrode (area = 0.00787 cm^2) in acetonitrile (0.1 M Bu_4NPF_6), at a scan rate of 100 mV s^{-1} over the potential range of -0.2 to 1.2 V vs Ag/AgCl, exhibits four well resolved diffusion-controlled one-electron processes labelled I to IV in Fig. 4a. The magnitudes of the peak currents for processes I and

III are similar and approximately double that observed for processes II and IV. The cyclic voltammetric data for processes I-IV as a function of scan rate are presented in Table S1 and Fig. S11.

Cyclic voltammetric data have been reported for $[Fe^{III}(L^{-})_2][TCNQF_4^{\bullet -}]$[23] and $[Fe^{II}(L^{\bullet})_2](BF_4)$[17] and on this basis, processes I and III are assigned to reduction of the $TCNQF_4^{\bullet -}$ anion to $TCNQF_4^{2-}$ and its oxidation to $TCNQF_4^{0}$, respectively. Processes II and IV arise from the oxidation and reduction reactions, respectively, of the nitroxide based cation $[Fe^{II}(L^{\bullet})_2]^{2+}$. The mid-point potentials ($E_m = (E_p^{ox} + E_p^{red})/2$) for each process I to IV are $E_{m\,I} = 0.03$ V, $E_{m\,II} = 0.26$ V, $E_{m\,III} = 0.55$ V and $E_{m\,IV} = 1.03$ V vs Ag/Ag^+. The peak-to-peak separation ΔE_p ($\Delta E_p = E_p^{ox} - E_p^{red}$) values are close to theoretically predicted values of 56 mV anticipated for one-electron electrochemically reversible couple at 23 °C.[31] A steady-state voltammogram of **1** obtained at a Pt microdisc electrode over the potential range of -0.3 to +1.5 V vs Ag/Ag^+ is shown in Fig. 4b. The current for each process relative to the zero current value is highlighted in this figure. The magnitude of the currents for processes I and III are similar to each other and close to twice those of processes II and III. The half-wave potential ($E_{1/2}$) values for the processes I to IV are identical to the mid-point potential values within experimental uncertainty. Since the current for process I is negative, this is assigned to the reduction of $TCNQF_4^{\bullet -}$ to $TCNQF_4^{2-}$ as shown in equation (1). The zero current passes through process II, but is predominantly a reduction current. Thus this process corresponds to the reduction of $[Fe^{II}(L^{\bullet})_2]^{2+}$ to the mixed valence $[Fe^{II}(L^{\bullet})(L^{-})]^{+}$ species which can undergo metal-ligand charge transfer to give the thermodynamically more stable $[Fe^{III}(L^{-})_2]^{+}$ species.[17,23] The positive component of the process II current

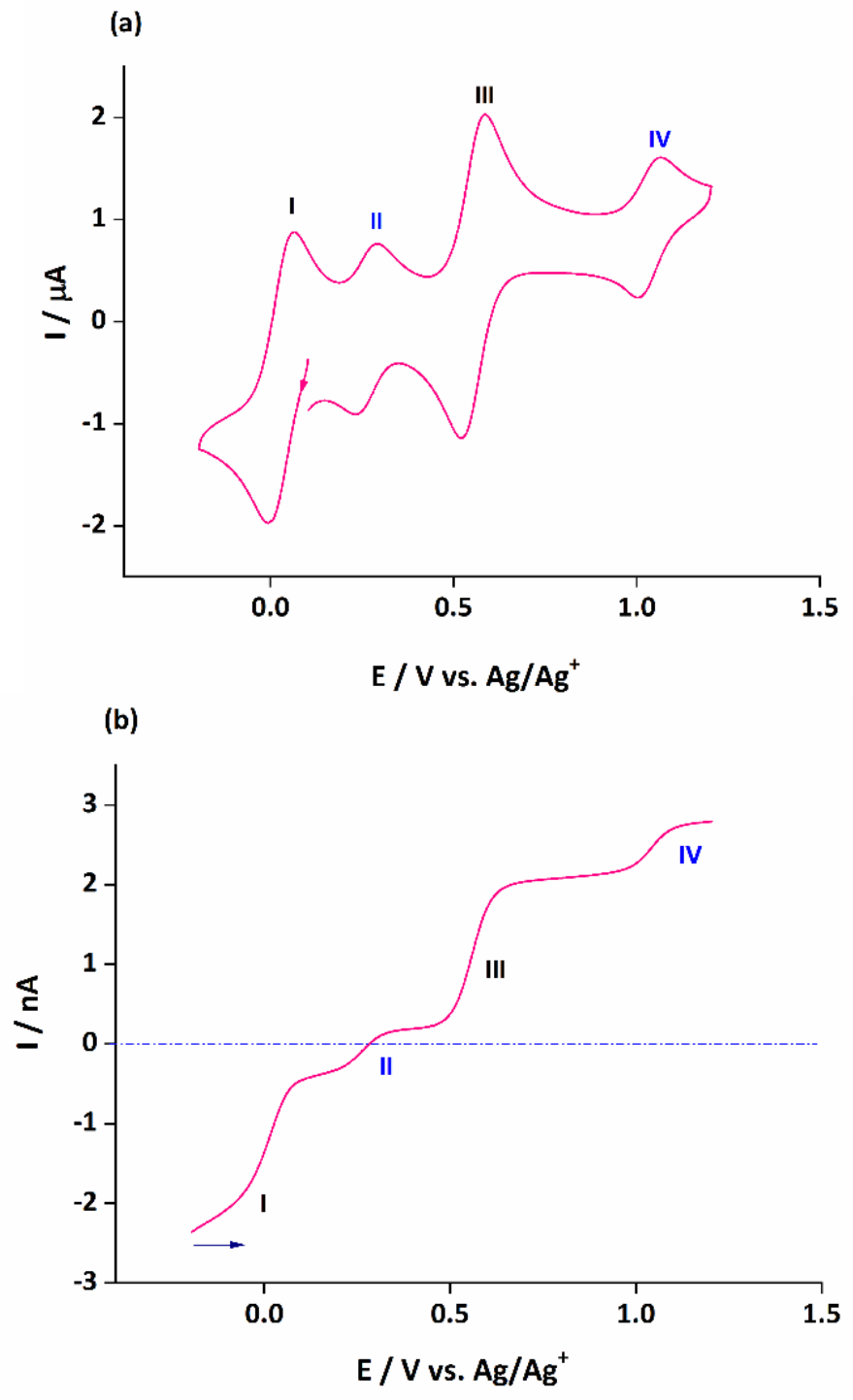

Fig. 4. (a) Transient cyclic voltammogram of 0.35 mM **1** obtained at a glassy carbon macrodisc electrode (A= 0.00787 cm^2) with a scan rate of 100 mVs^{-1} in CH_3CN (0.1 M Bu_4NPF_6). (b)

Steady-state voltammogram of 0.35 mM **1** obtained at a Pt microdisc electrode (10µM diameter) with a scan rate of 20 mVs^{-1} in CH_3CN (0.1 M Bu_4NPF_6).

$TCNQF_4^{\bullet-} + e^- \rightleftharpoons TCNQF_4^{2-}$ $\quad E_{m\,I} = 0.03V$ (1)

$[Fe^{II}L^{\bullet}_2]^{2+} + e^- \rightleftharpoons [Fe^{III}(L^-)_2]^+$ $\quad E_{m\,II} = 0.26V$ (2)

(via $[Fe^{II}(L^{\bullet})(L^-)]^+$ as in Scheme 1)

$TCNQF_4^{\bullet-} \rightleftharpoons TCNQF_4^{0} + e^-$ $\quad E_{m\,III} = 0.55V$ (3)

$[Fe^{II}L^{\bullet}_2]^{2+} \rightleftharpoons [Fe^{III}L^{\bullet}_2]^{3+} + e^-$ $\quad E_{m\,IV} = 1.03V$ (4)

suggests that a small amount of this reduced species $[Fe^{III}(L^-)_2]^+$ is present in the solution which gives rise to an oxidation current to give $[Fe^{II}(L^{\bullet})_2]^{2+}$. The origin of $[Fe^{III}(L^-)_2]^+$ present in the bulk solution is possibly due to reaction of $[Fe^{II}(L^{\bullet})_2]^{2+}$ with water, light or an unknown reductant, but the solution can be fully reduced to $[Fe^{III}(L^-)_2]^+$ by bulk electrolysis at the appropriate potential (see below). The redox reactions associated with process II are consistent with the square scheme shown in Scheme 1. Process III exhibits a positive current which corresponds to the one-electron oxidation of $TCNQF_4^{\bullet-}$ to $TCNQF_4^0$ as shown in equation (3). On the basis of the previous studies, process IV is assigned to the metal based oxidation of $[Fe^{II}(L^{\bullet})_2]^{2+}$ to $[Fe^{III}(L^{\bullet})_2]^{3+}$ as shown in equation (4).

An investigation of more negative potential region revealed a further reduction process V with $E_{m\,V}$ = -0.81 V vs Ag/Ag^+ as shown in the transient cyclic voltammogram in Fig. 5 (a) and the steady-state voltammogram in Fig. 5 (b). Process V is an electrochemically reversible one-electron reduction corresponding to the reduction of $[Fe^{III}(L^-)_2]^+$ cation to neutral $[Fe^{II}(L^-)_2]$, as shown in equation (5). This process is consistent with the one reported at a similar potential in the electrochemical study of $[Fe^{II}(L^{\bullet})_2][BF_4]_2$.[17]

$[Fe^{III}(L^-)_2]^+ + e^- \rightleftharpoons [Fe^{II}(L^-)_2]$ $\quad E_{m\,V} = -0.81V$ (5)

Complete removal of dissolved oxygen is required for the detection of process V. In a previous study two other reduction processes, labelled VI and VII were reported[23] in the Supporting

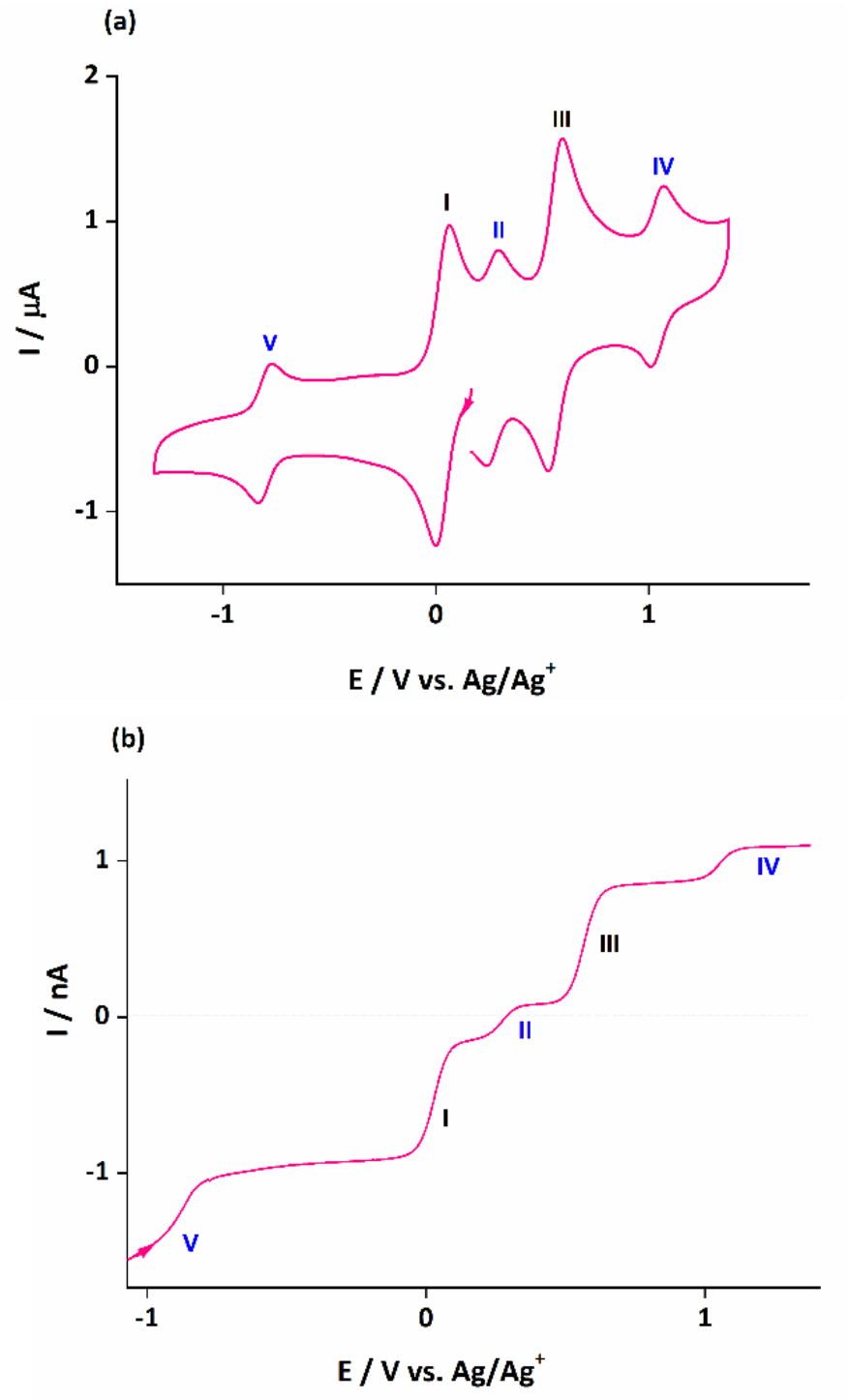

Fig. 5. (a) Transient cyclic voltammogram of 0.16 mM **1** obtained at a glassy carbon macrodisc electrode (A= 0.00787 cm^2) with a scan rate of 100 mVs^{-1} in CH_3CN (0.1 M Bu_4NPF_6). (b) Steady-state voltammoram of 0.16 mM **1** obtained at a Pt microdisc electrode (10 µM

diameter) with a scan rate of 20 mVs^{-1} in CH_3CN (0.1 M Bu_4NPF_6). Arrows show the initial scan direction.

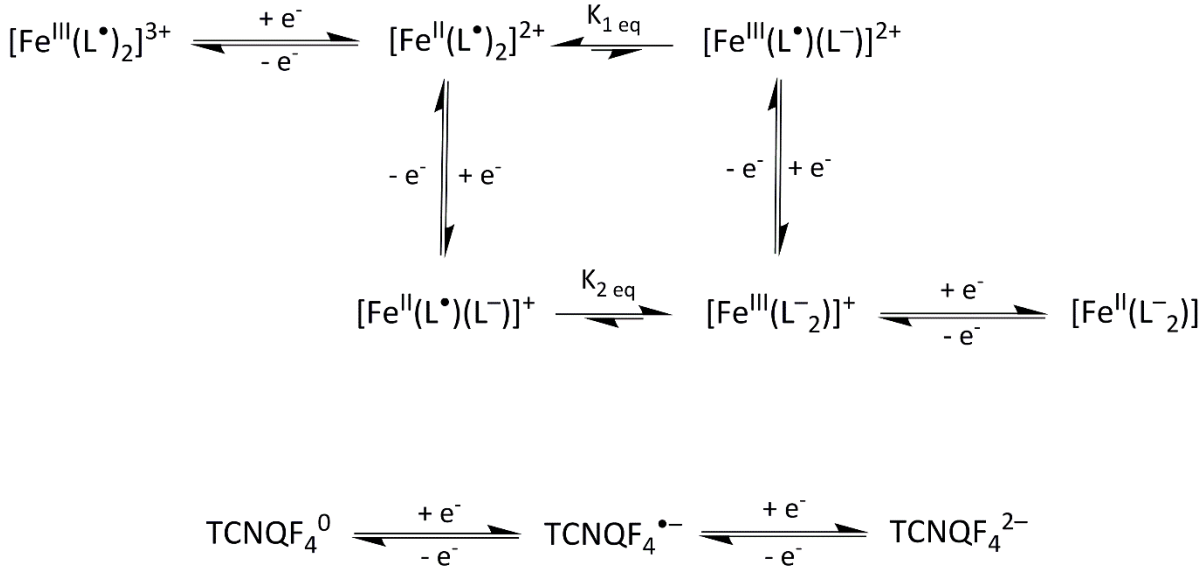

Scheme 1. Schematic representation of the reaction pathways associated with processes I-V for **1**.

Information for $[Fe^{III}(L^-)_2][TCNQF_4^{\bullet -}]$, however, these have now been shown to arise from the presence of dissolved oxygen.

After taking all the redox processes into the account, the overall reaction pathway associated with the electrochemical behaviour of **1** can be summarised in Scheme 1.

The ratio of close to 2:1 for the magnitudes of the peak and steady-state limiting currents for processes (I and II) : (II, IV and V) in the voltammetry of **1** is consistent with dissociation of the complex upon dissolution in CH_3CN as shown in equation (6).

$$[Fe^{II}L^{\bullet}_2](TCNQF_4^{\bullet -})_{2\ (solid)} \xrightarrow{CH_3CN} [Fe^{II}L^{\bullet}_2]^{2+}_{(CH_3CN)} + 2\ TCNQF_4^{\bullet -}{}_{(CH_3CN)} \qquad (6)$$

A comparison of the voltammetry of $[Fe^{III}(L^{-})_2][TCNQF_4^{\bullet -}]$[23] and $[Fe^{II}(L^{\bullet})_2][TCNQF_4^{\bullet -}]_2$ (1)

A comparison of transient and steady-state voltammograms of $[Fe^{III}(L^{-})_2][TCNQF_4^{\bullet -}]$ and $[Fe^{II}(L^{\bullet})_2][TCNQF_4^{\bullet -}]_2$ is shown in Figs. 6 (a) and (b). Clearly in $[Fe^{II}(L^{\bullet})_2][TCNQF_4^{\bullet -}]_2$ the relative concentration of $TCNQF_4^{\bullet -}$ is twice that found in $[Fe^{III}(L^{-})_2][TCNQF_4^{\bullet -}]$ and this is reflected in the relative peak magnitudes of the processes I and III vs II and IV. Except for this feature, the transient cyclic voltammograms are very similar for the dissolved forms of each compound. However, interestingly the position of process II relative to the zero current differs in the steady-state voltammograms for each compound and this reflects the difference in their redox states as shown in Fig. 6 (b). Chemical synthesis gave a mixture of both cations as identified by the location of the zero current with respect to process II. Thus as anticipated depending on the relative concentrations of $[Fe^{II}(L^{\bullet})_2]^{2+}$ and $[Fe^{III}(L^{-})_2]^{+}$ a slight deviation in the position of zero current is observed with respect to process II (see Fig. 6 (b)). If we have pure $[Fe^{III}(L^{-})_2]^{+}$ it would be predicted to give only oxidation current and similarly, pure $[Fe^{II}(L^{\bullet})_2]^{2+}$ would only show a reduction current. This situation can be achieved by applying an appropriate potential under bulk electrolysis conditions (0.157 and 0.437 V vs Ag/Ag^{+}, respectively) to the emerald green coloured solution of $[Fe^{II}(L^{\bullet})_2][TCNQF_4^{\bullet -}]_2$ as shown in Fig. S12. No change in the solution colour was observed after either bulk electrolysis experiment. Indeed a solution of only $[Fe^{III}(L^{-})_2]^{+}$ generates fully oxidation current with regard to process II to give $[Fe^{II}(L^{\bullet})_2]^{2+}$. Conversely, after bulk reductive electrolysis to give only $[Fe^{II}(L^{\bullet})_2]^{2+}$ cation in solution, the small oxidation current component seen in process II and attributed to the presence of some $[Fe^{III}(L^{-})_2]^{+}$ in the bulk solution, as shown in Fig. 4 (b), is now removed. As expected, processes I, III, IV and V remain intact after such oxidative or reductive bulk electrolysis experiments.

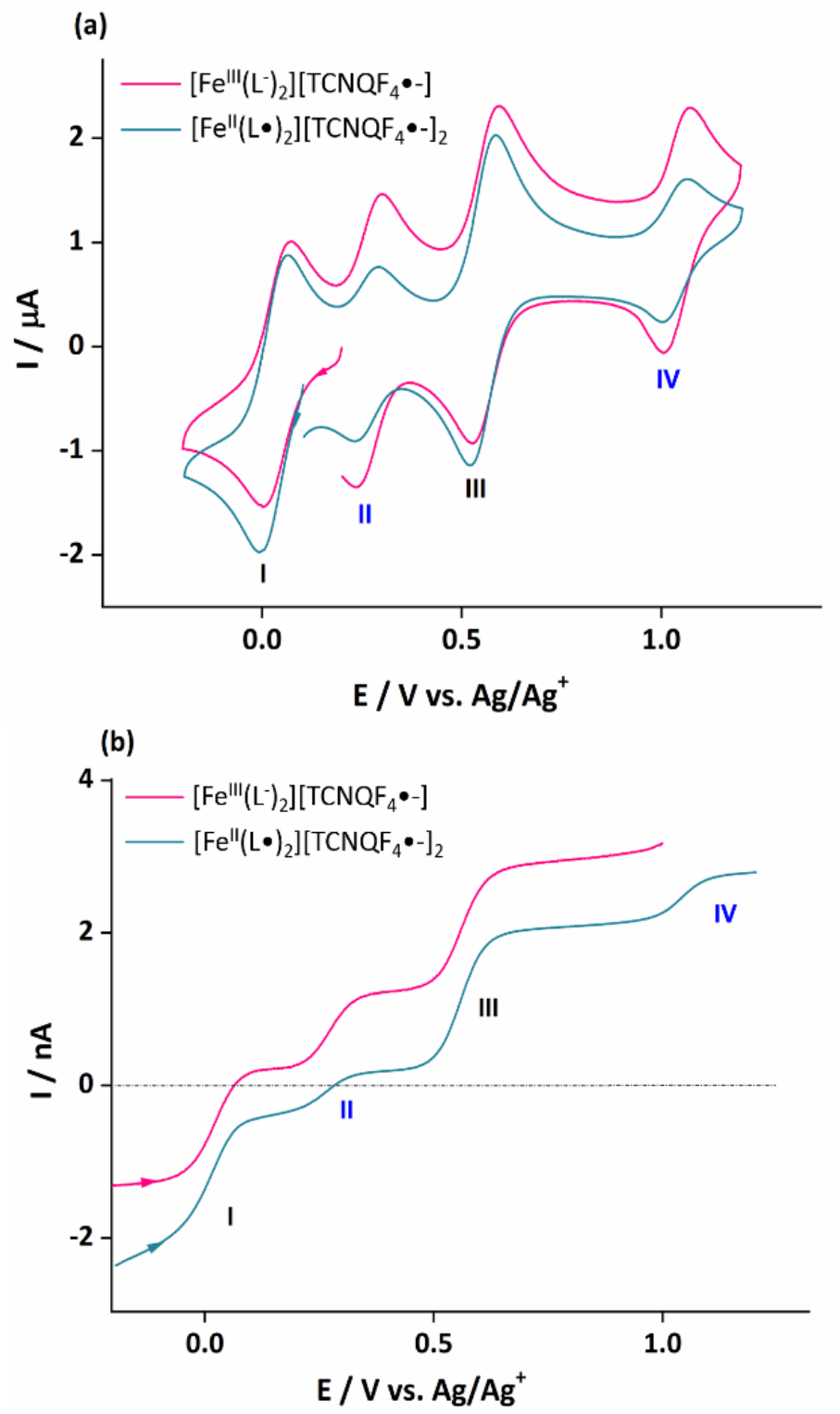

Fig. 6. A comparison of (a) transient cyclic voltammograms and (b) steady-state voltammograms of $[Fe^{III}(L^{-})_2][TCNQF_4^{\bullet -}]$ and $[Fe^{II}(L^{\bullet})_2][TCNQF_4^{\bullet -}]_2$ (**1**) systems in acetonitrile (0.1 M Bu_4NPF_6).

Nevertheless, during these bulk electrolysis experiments, it was noted that the position where zero current passes through process II is slightly dependent on the direction of the scan and also the initial potential. This is attributed to the influence of the thermodynamically favoured cross redox reactions that can occur. For example when the initial potential is set at -0.2 V vs Ag/Ag^{+}, $TCNQF_4^{2-}$ is generated.

Conclusion

Previous work on reacting $[Fe^{II}(L^{\bullet})_2][BF_4]_2$ with Li_2TCNQF_4 resulted in $[Fe^{III}(L^{-})_2][TCNQF_4^{\bullet-}]$ where $TCNQF_4^{2-}$ oxidised to the $TCNQF_4^{\bullet-}$ radical anion and in the process converted $[Fe^{II}(L^{\bullet})_2]^{2+}$ to $[Fe^{III}(L^{-})_2]^{+}$ via a reductively induced oxidation process.[23] In this work we have sought confirmation of the hypothesis that the $TCNQF_4^{2-}$ anion is solely responsible for the above redox process by investigating the related reaction involving $LiTCQNF_4$ instead of Li_2TCNQF_4. The central idea is that by using $LiTCNQF_4$ in a similar reaction to that used above the two BF_4 anions in $[Fe^{II}(L^{\bullet})_2][BF_4]_2$ should simply be replaced by two $TCNQF_4^{\bullet-}$ radical anions in a metathesis reaction resulting in a new, but related, material. Single crystal X-ray diffraction measurements; Raman, FTIR and UV-Vis spectroscopy studies; and solution based electrochemistry have confirmed that the metathesis has taken place resulting in the formation of $[Fe^{II}(L^{\bullet})_2][TCNQF_4^{\bullet-}]_2{\cdot}2CH_3CN$ (**1**). The data above are self-consistent and appropriate for the assignment of a central low-spin Fe^{II} ion; the neutral radical form ($L^{\bullet}$) of the ligand; and the presence of the radical anion, $TCNQF_4^{\bullet-}$. The strong antiferromagnetic exchange between the two radical ligands and between stacked pairs of eclipsed $TCNQF_4^{\bullet-}$ radical anions results in a largely diamagnetic material but one that shows rich electrochemistry with five one electron, reversible, well resolved, diffusion-controlled

processes. This highlights the utility of the different redox forms of $TCNQF_4$ in inorganic synthesis and in the preparation of redox-active multifunctional materials.

Experimental

General Considerations $[Fe^{II}(L^{\bullet})_2][BF_4]_2$ and 4,4-dimethyl-2,2-di(2-pyridyl) oxazolidine *N*-oxide ($L^{\bullet}$) were synthesised as described previously.[17] $LiTCNQF_4$ was prepared according to a literature preparation.[32] All other reagents and solvents were of reagent grade and used as received. Microanalyses were performed by MEDAC Ltd.

Syntheses.

$[Fe^{II}(L^{\bullet})_2][TCNQF_4^{\bullet-}]_2 \cdot 2CH_3CN$ (1) 10 mg (0.013 mmol) of $[Fe^{II}(L^{\bullet})_2][BF_4]_2$ was dissolved in a mixture of 2.5 ml acetonitrile and 0.5 ml dichloromethane. Then 1.0 ml of a methanolic solution containing 7.3 mg (0.026 mmol) of $LiTCNQF_4$ was added and this mixture left open to the air to crystallise. X-ray quality dark green crystals formed after 5 days in reasonable yield. Yield 11 mg (69.0%). Anal. Calcd (%) for **1**, $C_{58}H_{38}N_{16}O_4F_8Fe$ ($[Fe^{II}(L^{\bullet})_2][TCNQF_4^{\bullet-}]_2 \cdot 2CH_3CN$): C, 56.6; H, 3.11; N, 18.21. Found: C, 56.01; H, 3.22; N, 18.10. FTIR (ATR cm^{-1}): 2194s, 2173s, 1640w, 1611s, 1536m, 1505w, 1487s, 1470m, 1446w, 1390s, 1346w, 1335w, 1317w, 1302w, 1280w, 1240s, 1200w, 1159w, 1141w, 1084s, 1031w, 1009w, 999w, 980m, 968s, 928w, 908w, 881w, 831w, 771s, 713w, 674w, 654m (Fig. S1). For Raman spectra see Fig. S2.

X-ray Crystallography. X-ray crystallographic measurements were performed on **1** at 123(2) K using a Bruker Smart Apex X8 diffractometer with Mo-Kα radiation (λ = 0.7107 Å). Single crystals were mounted on a glass fibre with refinement parameters and crystallographic data found in Table 4. This was solved by direct methods (SHELXS-97),

and refined (SHELXL-97) by full least-squares on all F^2 data.[33] In **1** the asymmetric unit contains half the iron monomer, one $TCNQF_4^{\bullet -}$ monoanion and one solvate acetonitrile molecule. All non-hydrogen atoms are refined anisotropically and all hydrogens placed in calculated positions. Full crystallographic data and selected bond lengths and angles can be found in Table 4 and Table 1. CCDC number 1508568.

Table 4 Crystallographic data for **1**.

Parameters	**1**
Formula	$C_{58}H_{38}N_{16}O_4F_8Fe$
M_r	1230.89
Crystal System	Monoclinic
Space Group	C2/c
a /Å	21.9574(7)
b /Å	16.2749(7)
c /Å	15.7265(6)
α /°	90
β /°	108.080(2)
γ /°	90
V / Å^3	5342.4
T / K	123(2)
Z	4
ρ_{calcd} / g cm^{-3}	1.530
λ[a] / Å	0.71073
Ind. reflns	7504
Reflns with $I > 2\sigma(I)$	5963
Parameters	397
Restraints	0
Final *R*1, *wR*2[b] [$I > 2\sigma(I)$]	0.0555, 0.1258
*R*1, *wR*2[b] all data	0.0732, 0.1346
Goodness of fit	1.116
Largest residuals/ e Å^{-3}	0.826, -1.313

[a] Graphite monochromators. [b] $R1 = \Sigma \mid |F_o| - |F_c| \mid / \Sigma |F_o|$, $wR2 = \{\Sigma[w(F_o^2 \Sigma F_c^2)^2]/\Sigma[w(F_o^2)]\}^{1/2}$.

Electrochemistry. A three-electrode electrochemical cell was used to perform the electrochemical experiments at ambient temperatures of 23±2°C with a Bioanalytical Systems (West Lafayette, IN) BASi Epsilon-EC electrochemical workstation. A glassy carbon (GC) macrodisc electrode (area = 0.00787 cm^2) or a platinum (Pt) microelectrode (10 µm diameter)

were employed as the working electrodes, along with Ag/Ag^+ (Ag wire in contact with acetonitrile containing 0.1 M $AgNO_3$ and 0.1 M Bu_4NPF_6) as the standard reference electrode and platinum wire as the counter electrode in voltammetric studies. The Ag/Ag^+ (0.1 M $AgNO_3$) reference electrode had a potential of 0.366 V vs $Fc^{0/+}$ (Fc = Ferrocene). Bulk electrolysis experiments were performed with a three electrode cell with a large area Pt mesh working electrode, Pt gauze as the counter electrode and a Ag/Ag^+ reference electrode (as described above) with each compartment being separated by a glass frit. All solutions were degassed with nitrogen for 10 min prior to undertaking electrochemical experiments.

Infrared and Raman Spectroscopy. FTIR spectra were recorded using a Spectrac Diamond ATR instrument. Raman spectra were acquired with a Renishaw Raman RM2000 spectrometer and microscope using a laser strength of 18mW at a wavelength of 514 nm.

Magnetic Susceptibility Measurements. Variable-temperature magnetic susceptibility measurements were performed on a Quantum Design MPMS 7T SQUID magnetometer over the temperature range 2 - 300 K for **1** in an applied DC field of 0.1 T. The SQUID magnetometer was calibrated by use of a standard palladium sample (Quantum Design) of accurately known magnetization or by use of magnetochemical calibrants such as $CuSO_4 \cdot 5H_2O$. Crystals of **1** were collected and these were dispersed in Vaseline in order to avoid torqueing. The sample mulls were contained in a calibrated capsule held at the centre of a drinking straw that was fixed at the end of the sample rod.

Supplementary Material

Molecular structure (Fig. S1) and packing figures (Fig. S2); Raman (Fig. S3-S4) and FTIR spectra (Fig. S5); $\chi_M T$ vs T plots (S6-S8); UV-Vis spectra (Fig. S9-S10); cyclic voltammetric data at

various scan rates (Table S1 and Fig. S11) and further steady state voltammetric data (Fig. S12) are available on the journals website.

Acknowledgments

K.S.M thanks the Australian Research Council for a discovery grant DP 140101013. L.L.M and A.M.B would like to thank the Australian Research Council for the Discovery Grants DP120101066 and DP170103477. I.A.G thanks the University of Brighton for the output enhancement fund.

Conflicts of Interest

The authors declare no conflicts of interest.

References

[1] W. Kaim, B. Schwederski, *Coord. Chem. Rev*. **2010**, *254*, 1580. doi:10.1016/j.ccr.2010.01.009

[2] J. J. Weiss, *Nature* **1964**, *202*, 83. doi:10.1038/202083b0

[3] L. Pauling, *Nature* **1964**, *203*, 182. doi:10.1038/203182b0

[4] K. L. Bren, R. Eisenberg, H. B. Gray, *Proc. Natl. Acad. Sci.* **2015**, *112*, 13123. doi:10.1073/pnas.1515704112

[5] T. Borowski, P. E. M. Siegbahn, *J. Am. Chem. Soc.* **2006**, *128*, 12941. doi:10.1021/ja0641251

[6] M. Y. M. Pau, M. I. Davis, A. M. Orville, J. D. Lipscomb, E. I. Solomon, *J. Am. Chem. Soc*. **2007**, *129*, 1944. doi:10.1021/ja065671x

[7] K. D. Sutherlin, Y. Wasada-Tsutsui, M. M. Mbughuni, M. S. Rogers, K. Park, L. V. Liu, Y. Kwak, M. Srnec, L. H. Böttger, M. Frenette, Y. Yoda, Y. Kobayashi, M. Kurokuzu, M.

Saito, M. Seto, M. Hu, J. Zhao, E. E. Alp, J. D. Lipscomb, E. I. Solomon, *J. Am. Chem. Soc*. **2018**, *140*, 16495. doi:10.1021/jacs.8b06517

[8] A. W. Rutherford, A. Boussac, P. Faller, *Biochim. Biophys. Acta* **2004**, *1655*, 222. doi:10.1016/j.bbabio.2003.10.016

[9] R. E. Cowley, J. Cirera, M. F. Qayyum, D. Rokhsana, B. Hedman, K. O. Hodgson, D. M. Dooley, E. I. Solomon, *J. Am. Chem. Soc.* **2016**, *138*, 13219. doi:10.1021/jacs.6b05792

[10] B. L. Greene, A. T. Taguchi, J. Stubbe, D. G. Nocera, *J. Am. Chem. Soc.* **2017**, *139*, 16657. doi:10.1021/jacs.7b08192

[11] C. J. Gartshore, D. W. Lupton, *Adv. Synth. Catal*. **2010**, *352*, 3321. doi:10.1002/adsc.201000627

[12] Q. Cao, L. M. Dornan, L. Rogan, N. L. Hughes, M. J. Muldoon, *Chem. Commun*. **2014**, *50*, 4524. doi:10.1039/C3CC47081D

[13] B. L. Ryland, S. S. Stahl, *Angew. Chemie Int. Ed*. **2014**, *53*, 8824. doi:10.1002/anie.201403110

[14] P. J. Chirik, K. Wieghardt, *Science* **2010**, *327*, 794. doi:10.1126/science.1183281

[15] A. Caneschi, D. Gatteschi, R. Sessoli, P. Rey, *Acc. Chem. Res*., **1989**, *22*, 392. doi:10.1021/ar00167a004

[16] A. Caneschi, D. Gatteschi, P. Rey, *Prog. Inorg. Chem*. **1991**, *39*, 331. doi:10.1002/9780470166406.ch6

[17] I. A. Gass, C. J. Gartshore, D. W. Lupton, B. Moubaraki, A. Nafady, A. M. Bond, J. F. Boas, J. D. Cashion, C. Milsmann, K. Wieghardt, K. S. Murray, *Inorg. Chem*. **2011**, *50*, 3052. doi:10.1021/ic102588h

[18] I. A. Gass, S. Tewary, A. Nafady, N. F. Chilton, C. J. Gartshore, M. Asadi, D. W. Lupton, B. Moubaraki, A. M. Bond, J. F. Boas, S. X. Guo, G. Rajaraman, K. S. Murray, *Inorg. Chem*., **2013**, *52*, 7557. doi:10.1021/ic400565h

[19] S. Tewary, I. A. Gass, K. S. Murray, G. Rajaraman, *Eur. J. Inorg. Chem*. **2013**, 1024. doi:10.1002/ejic.201201077

[20] I. A. Gass, S. Tewary, G. Rajaraman, M. Asadi, D. W. Lupton, B. Moubaraki, G. Chastanet, J.-F. Létard, K. S. Murray, Inorg. Chem. **2014**, *53*, 5055. doi:10.1021/ic5001057

[21] I. A. Gass, M. Asadi, D. W. Lupton, B. Moubaraki, A. M. Bond, S.-X. Guo, K. S. Murray, *Aust. J. Chem*. **2014**, *67*, 1618. doi:10.1071/CH14390

[22] A. H. Pedersen, B. L. Geoghegan, G. S. Nichol, D. W. Lupton, K. S. Murray, J. Martínez-Lillo, I. A. Gass, E. K. Brechin, Dalton. Trans. **2017**, *46*, 5250. doi:10.1039/C7DT00752C

[23] I. A. Gass, J. Lu, M. Asadi, D. W. Lupton, C. M. Forsyth, B. L. Geoghegan, B. Moubaraki, J. D. Cashion, L. L. Martin, A. M. Bond, K. S. Murray, *Chempluschem* **2018**, *83*, 658. doi:10.1002/cplu.201800010

[24] T. J. Emge, M. Maxfield, D. O. Cowan, T. J. Kistenmacher, *Mol. Cryst. Liq. Cryst*., **1981**, *65*, 161. doi:10.1080/00268948108082132

[25] S. A. O'Kane, R. Clérac, H. Zhao, X. Ouyang, J. R. Galán-Mascarós, R. Heintz, K. R. Dunbar, J. Solid State Chem. **2000**, *152*, 159. doi: 10.1006/jssc.2000.8679

[26] T. H. Le, J. Lu, A. M. Bond, L. L. Martin, *Inorg. Chim. Acta* **2013**, *395*, 252. doi:10.1016/j.ica.2012.10.019

[27] A. L. Sutton, B. F. Abrahams, D. M. D'Alessandro, R. W. Elliott, T. A. Hudson, R. Robson, P. M. Usov, *CrystEngComm* **2014**, *16*, 5234. doi:10.1039/C4CE00289J

[28] N. L. Haworth, J. Lu, N. Vo, T. H. Le, C. D. Thompson, A. M. Bond, L. L. Martin, Chempluschem **2014**, *79*, 962. doi:10.1002/cplu.201402013

[29] P. J. Kunkeler, P. J. van Koningsbruggen, J. P. Cornelissen, A. N. van der Horst, A. M. van der Kraan, A. L. Spek, J. G. Haasnoot, J. Reedijk, *J. Am. Chem. Soc*. **1996**, 118, 2190. doi:10.1021/ja943960s

[30] N. F. Chilton, R. P. Anderson, L. D. Turner, A. Soncini, K. S. Murray, *J. Comput. Chem*. **2013**, *34*, 1164. doi:10.1002/jcc.23234

[31] A. J. Bard, R. L. Faulkner, *Electrochemical Methods: Fundamentals and Applications* **2001** (Wiley & Sons, New York, 2nd edition).

[32] J. Lu, T. H. Le, D. A. K. Traore, M. Wilce, A. M. Bond, L. L. Martin, J. Org. Chem., 2012, 77, 10568–10574. doi: 10.1021/jo301403v

[33] G. M. Sheldrick, SHELX-97, Program for the solution and refinement of crystal structures, University of Göttingen, Germany, 1997.